

UNCLASSIFIED

AD NUMBER
AD903553
NEW LIMITATION CHANGE
TO Approved for public release, distribution unlimited
FROM Distribution authorized to U.S. Gov't. agencies only; Test and Evaluation; MAY 1972. Other requests shall be referred to Commanding Officer, Frankford Arsenal, ATTN: SMUFA-L3200, Philadelphia, PA 19137.
AUTHORITY
USA PA, per DTIC Form 55, dtd 25 may 2011

THIS PAGE IS UNCLASSIFIED

AD903553 7

REPORT M72-11-1

AD

A FRACTOGRAPHIC INVESTIGATION OF EXPLOSIVELY FRAGMENTED SILICON-MANGANESE STEELS BY SCANNING ELECTRON MICROSCOPY

by

JAMES C. BEETLE  
WILLIAM B. STEWARD

DDC  
RECEIVED  
SEP 27 1972  
D

May 1972

Distribution is limited to U. S. Government agencies only - Test and Evaluation, May 1972. Other requests for this document must be referred to the Commanding Officer, Frankford Arsenal, Philadelphia, Pa., 19137, Attn: SMUFA-L3200.



**DEPARTMENT OF THE ARMY  
FRANKFORD ARSENAL  
Philadelphia, Pa. 19137**

DISPOSITION INSTRUCTIONS

Destroy this report when it is no longer needed. Do not return it to the originator.

The findings in this report are not to be construed as an official Department of the Army position unless so designated by other authorized documents.

REPORT M72-11-1

A FRACTOGRAPHIC INVESTIGATION OF EXPLOSIVELY FRAGMENTED  
SILICON-MANGANESE STEELS BY SCANNING ELECTRON MICROSCOPY

by

JAMES C. BEETLE  
WILLIAM B. STEWARD

AMCMS Code: 502E.11.09900  
DA Project: 1T062105A039

Distribution is limited to U.S. Government agencies only - Test and Evaluation, May 1972. Other requests for this document must be referred to the Commanding Officer, Frankford Arsenal, Philadelphia, Pa., 19137, Attn: SMUFA-L3200.

Pitman-Dunn Research Laboratory  
FRANKFORD ARSENAL  
Philadelphia, Pa. 19137

May 1972

## ABSTRACT

The influence of microstructure upon fracture mode and relative fragmentation performance of steel test cylinders was assessed fractographically by scanning electron microscopy. For the compositions used in this study, a microstructural constituent which provides a path for brittle fracture under dynamic conditions appears to be a necessity for enhanced fragmentation.

## TABLE OF CONTENTS

	<u>Page No.</u>
INTRODUCTION . . . . .	1
MATERIALS AND EXPERIMENTAL PROCEDURE . . . . .	2
RESULTS . . . . .	5
SEM of XF-1 Steel . . . . .	5
SEM of HF-1 Steel . . . . .	13
SEM of Fracture Surfaces Adjacent to Inner Walls of Cylinders . . . . .	14
DISCUSSION . . . . .	25
SEM of XF-1 Steel . . . . .	25
SEM of HF-1 Steel . . . . .	26
SEM of Fracture Surfaces Adjacent to Inner Walls of Cylinders . . . . .	27
CONCLUSIONS . . . . .	27
RECOMMENDATIONS . . . . .	28
REFERENCES . . . . .	29
DISTRIBUTION . . . . .	30

### List of Illustrations

Figure

1. Schematic Illustrating Various Surfaces of a Fragment . .	3
2. Schematic Illustrating Various Fracture Modes . . . . .	4
3. XF-1: Large Grained Ferrite Network and Coarse Pearlite Matrix, Radial Surface . . . . .	7
4. XF-1: Large Grained Ferrite Network and Coarse Pearlite Matrix (Same fragment as Figure 3, but an area closer to the center of the radial surface). . . . .	7
5. XF-1: Ferrite Network and Moderately Tempered Martensite Matrix, Axial Surface . . . . .	9

List of Illustrations (Cont'd)

<u>Figure</u>	<u>Page</u>
6. XF-1: Ferrite Network and Moderately Tempered Martensite Matrix (Same as Figure 5, but higher magnification) . . . .	9
7. XF-1: Ferrite Network and Fine Pearlite Matrix, Radial Surface . . . . .	11
8. HF-1: Carbide Network and Lightly Tempered Martensite Matrix, Radial Surface . . . . .	15
9. HF-1: Carbide Network and Lightly Tempered Martensite Matrix, Radial Surface (Same as Figure 8, but higher magnification) . . . . .	15
10. HF-1: Carbide Network and Fine Pearlite Matrix, Axial Surface . . . . .	17
11. HF-1: Carbide Network and Fine Pearlite Matrix, Axial Surface (Same as Figure 10, but higher magnification) . . . . .	17
12. HF-1: Spheroidized, Radial Surface . . . . .	19
13. HF-1: Spheroidized, Radial Surface (Same as Figure 12, but higher magnification) . . . . .	19
14. HF-1: Homogenized at 2200° F; Then Heat-Treated to Produce Random Carbides and Pearlite; Radial Surface . . . . .	21
15. HF-1: Homogenized at 2200° F; Then Heat Treated to Produce Random Carbides and Pearlite; Radial Surface (Same as Figure 14, but higher magnification) . . . . .	21
16. HF-1: Partial Carbide Network and Spheroids in a Well Tempered Martensite Matrix, Shear Surface . . . . .	23
17. HF-1: Partial Carbide Network and Spheroids in a Well Tempered Martensite Matrix, Shear Surface (Same as Figure 16, but higher magnification) . . . . .	23

List of Tables

<u>Table</u>	
I. Fragmentation Performance of Selected XF-1 Steel Cylinders with Selected Microstructures. . . . .	5
II. Fragmentation Performance of HF-1 Steel Cylinders with Selected Microstructures . . . . .	13

## INTRODUCTION

This report describes results of an initial attempt to correlate the fragmentation characteristics of two silicon-manganese steels with their fracture morphology using the scanning electron microscope (SEM).

It is generally conceded that the strength and relative ductility or brittleness of steels, as determined by conventional tensile and impact tests, are unreliable indicators of their fragmentation behavior under explosive loading. It appears, perhaps, that response to explosive fragmentation is structure-sensitive to such a degree that this effect partially overrides strength and ductility factors, thereby preventing any direct and consistent correlation between fragmentation behavior and mechanical properties.

A study was conducted by Bardes<sup>1</sup> in 1969 relating the microstructures of two silicon-manganese steels to their fragmentation behavior. Conventional metallographic techniques were used to delineate crack paths and to identify microstructural features in recovered fragments. Fracture modes and crack nucleation sites were inferred from the observations; however, microscopic examination of the fracture surfaces was not attempted.

Fragments recovered from explosively fragmented steel frequently exhibit extremely jagged fracture surfaces. Their topography is beyond the depth-of-field of optical microscopic equipment at other than very low magnifications but, in most instances, is well within the capability of the SEM over its range of useful magnifications (20X to 10,000X).

The direct identification of microscopic fracture modes using the SEM should permit a more complete and less ambiguous analysis of the fracture process than do the limited fractographic and indirect metallographic optical methods.

The SEM study described in the present report was undertaken to extend Bardes' concept of correlating fragmentation behavior with microstructure and fracture mode. The details of fracture morphology discernible by SEM techniques will hopefully provide a means for establishing a distinct relationship between various microstructural elements and their influence on the fragmentation of steel. The establishment of such a relationship could ultimately provide a basis for selection of steels for use in naturally fragmenting munitions.

---

<sup>1</sup>B.P. Bardes, "Mechanism of Fragmentation of Silico-Manganese Steels," Frankford Arsenal Report R-1918, March 1969.

## MATERIALS AND EXPERIMENTAL PROCEDURE

The materials used in this work were fragments from two steels whose fragmentation behavior had been characterized previously at Frankford Arsenal.<sup>1</sup> The steels were basically silicon-manganese steels - one, a hypoeutectoid and the other, a hypereutectoid composition. The former, designated as XF-1, contained 0.51% C, 1.63% Mn, and 0.81% Si. The latter, designated as HF-1, contained 1.10% C, 1.79% Mn, and 0.82% Si. Cylinders were fabricated from the two steels, heat-treated to provide a variety of microstructures, and fragmented using composition B explosive. Fragments were recovered by a water recovery method and separated into weight groups by standard screening techniques.

The present fractographic study was performed using SEM exclusively. It was limited in scope to examinations of fragments from cylinders of each composition which had demonstrated the best, an intermediate, and the worst fragmentation performance as judged by fragment count.

The microstructures of the HF-1 cylinders with the best and worst fragmentation ratings were quite different. Since a number of the HF-1 cylinders could be categorized as having an intermediate fragmentation rating, one with a microstructure dissimilar to those ranked best and worst was selected for SEM examination, to provide more information on the effect of structure on fracture mode.

The XF-1 cylinders with the best and worst fragmentation ratings, however, had a similarity in their microstructure. Although their matrix constituents were different, both possessed ferrite grain boundary networks. Because of this, the sample of XF-1 chosen to represent intermediate fragmentation behavior in the SEM study, was one which also exhibited a ferrite grain boundary network. It was anticipated that the fracture modes for cylinders with this hypoeutectoid composition would be attributable to the unlike matrix microstructures associated with the three ratings.

In each instance, representative fragments were chosen from size groups having average masses between 2 and 4 grains. These were of a convenient size for examining for macroscopic fracture morphology and could be mounted in multiples for SEM examination.

Three fracture surfaces of each fragment were examined wherever possible. A schematic illustrating the fracture surfaces is shown in Figure 1. The figure is intended to be descriptive only and does not necessarily depict a typically shaped fragment. The surface, radially

---

<sup>1</sup>B.P. Bardes, "Mechanism of Fragmentation of Silico-Manganese Steels," Frankford Arsenal Report R-1918, March 1969.

directed with respect to the cylinder axis, is labeled r.s.; the surface which is inclined at an angle of approximately  $45^\circ$  to the inner surface is essentially a shear surface and is labeled s.s.; and the surface which is normal to the cylinder axis is labeled a.s. Some of the fragments examined exhibited all three surfaces. In many instances, however, radial surfaces were absent and axial surfaces were ill-defined.

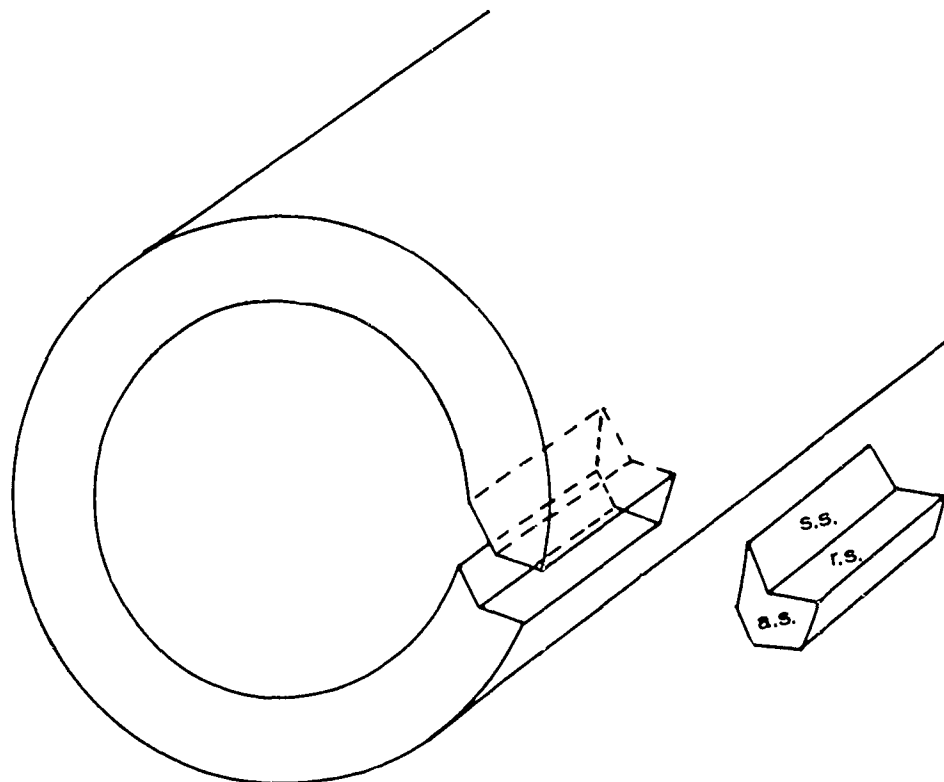
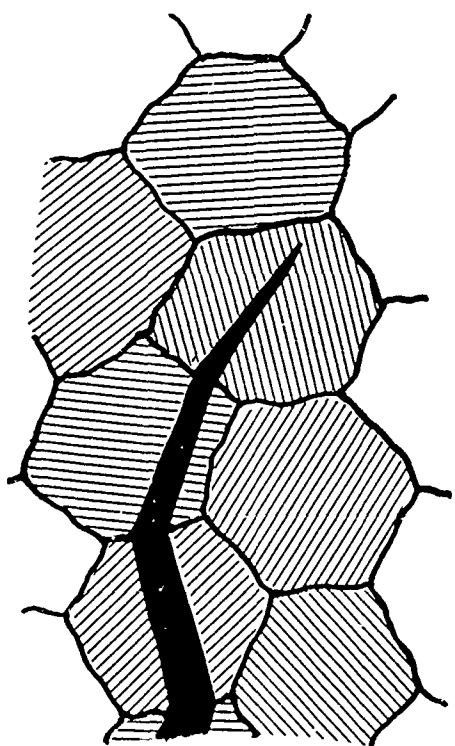


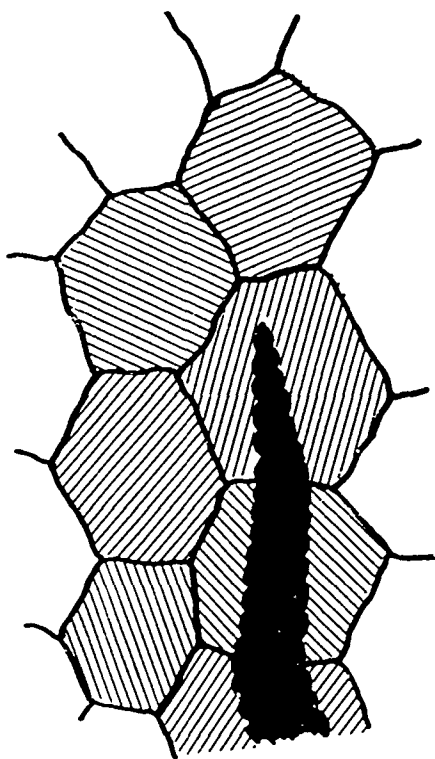
Figure 1. Schematic Illustrating Various Surfaces of a Fragment

A schematic illustrating various fracture modes often observed in fractographic studies is shown in Figure 2. They are introduced here to provide a basis for the discussion on the fractographs which will be presented for XF-1 and HF-1.

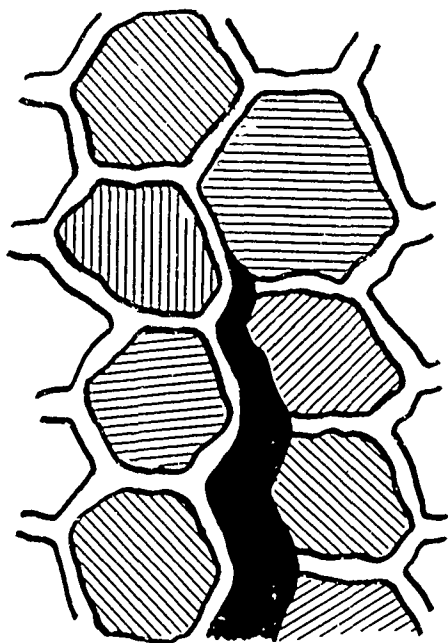
Intergranular separation (upper left) refers to the separation of a grain boundary constituent from the matrix. This is considered to be a relatively brittle fracture mode. Another brittle fracture mode is transgranular cleavage (upper right), in which fracture occurs along certain "cleavage planes" within a grain. The fracture surface exhibited by this fracture mode consists of relatively flat areas whose size corresponds to the grain size of the material, and is characterized by "river patterns" which are related to the direction of crack propagation.



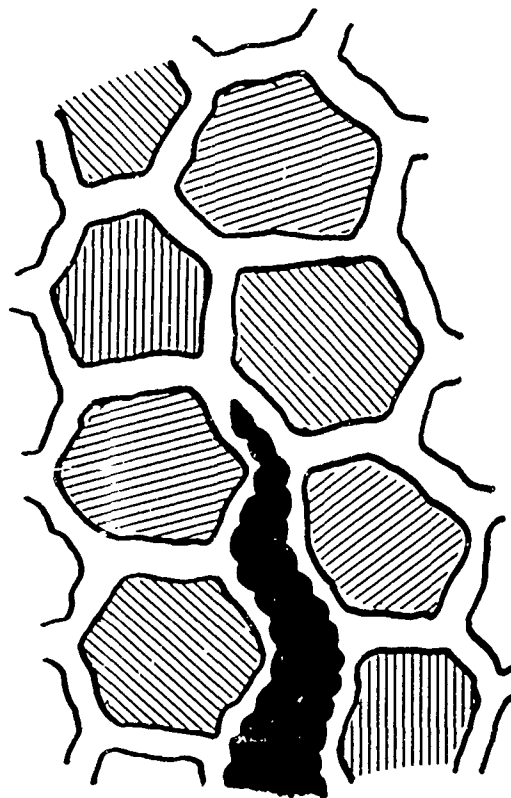
TRANSGRANULAR CLEAVAGE



TRANSGRANULAR DIMPLED



INTERGRANULAR SEPARATION



INTERGRANULAR DIMPLED

Figure 2. Schematic Illustrating Various Fracture Modes

The dimpled modes of fracture, shown in the lower section of the figure, are generally described as ductile modes. They absorb much more energy than the separation or cleavage modes. The intergranular dimpled mode (lower left) results from the ductile rupture of the grain boundary constituent. The transgranular dimpled mode also occurs by a ductile process but is unaffected by grain boundaries. It is usually associated with precipitates, inclusions, or regions of severe plastic flow.

## RESULTS

### SEM of XF-1 Steel

The microstructure, hardness, and fragmentation performance of three selected conditions of XF-1 examined in this study are indicated in Table I. The fragmentation performance is shown as  $N_{\frac{1}{2}}$ . These values were determined by Bardes<sup>1</sup> using Mott plot analysis. Higher values of  $N_{\frac{1}{2}}$  are generally considered to indicate better fragmentation performance. The results of the fractographic studies on the three conditions are described below. In each of the fractographs shown, the outer surface of the cylinder from which the fragment came would be toward the right.

Table I.  
Fragmentation Performance of Selected XF-1 Steel Cylinders  
With Selected Microstructures

<u>Structure</u>	<u>Hardness</u>	<u><math>N_{\frac{1}{2}}</math></u>
Large grained ferrite network and coarse pearlite matrix	Rc 20	393
Ferrite network and moderately tempered martensite matrix	Rc 37	217
Ferrite network and fine pearlite matrix	Rc 30	140

<sup>1</sup>B.P. Bardes, "Mechanism of Fragmentation of Silico-Manganese Steels," Frankford Arsenal Report R-1918, March 1969.

A SEM fractograph of the radial surface of a fragment from the best fragmenting condition of XF-1, is shown in Figure 3. In this condition, the microstructure of the XF-1 consists of a large grained ferritic network with a coarse pearlite matrix. The fractograph indicates a mixed mode of fracture consisting of both intergranular dimpled and transgranular cleavage modes. The latter is well demonstrated by noting the river pattern on the large facet which is slightly to the right of center of the fractograph. This facet is situated in an area corresponding to about the third grain from the outside surface of the cylinder. Note that the river pattern is fanning out from left to right. This indicates that crack propagation, within this area, was directed toward the outer surface of the cylinder. The intergranular dimpled mode of fracture is exhibited at regions to the left and above the center of the figure.

Figure 4 is a fractograph of the same fragment as that chosen in Figure 3, but represents an area closer to the center of the radial surface. A mixed mode of intergranular dimpled and transgranular cleavage is still apparent. However, here the convergence of lines within the river pattern indicates that crack propagation was directed away from the outside surface of the cylinder. This suggests that the radial fracture surface resulted from cracks nucleating within the cylinder wall, somewhere near the outer surface, and propagating toward the inner and outer surfaces of the cylinder.

The fracture mode observed for fragments from an XF-1 cylinder which exhibited intermediate fragmentation performance, was considerably different from that observed in the case of the best fragmenting XF-1 material. This is shown in Figure 5. The fracture mode observed here is predominantly of an intergranular dimpled nature with the grain structure elongated. The dimpled structure is shown more clearly at higher magnification in Figure 6. It should be noted that the microstructure of this material is quite different from that of the best fragmenting XF-1 material, which probably accounts for the large differences in fracture morphology. In this case, the microstructure consists of a smaller ferrite network and a matrix of martensite rather than pearlite. It should also be noted that none of the fragments with this structure exhibited fracture on radial surfaces.

The fracture mode that was observed on axial and radial surfaces of fragments from XF-1 cylinders with the poorest fragmentation is shown in Figure 7. The fracture is a mixed mode which consists of transgranular cleavage and isolated dimpled rupture at prior austenite grain boundaries. In comparison to the microstructure of the best XF-1, this structure consists of a finer ferrite network and a finer pearlite matrix.



$N_{\frac{1}{2}} = 398$

Mag: 300 $\lambda$

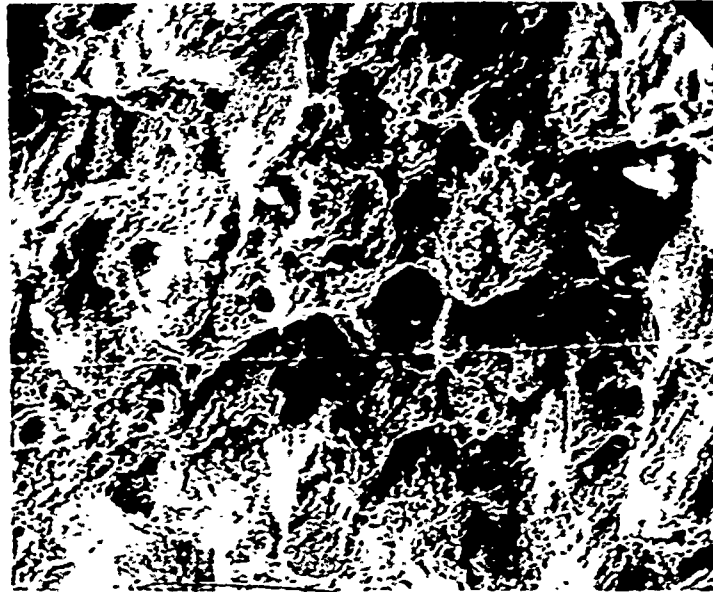
Figure 3. XF-1: Large Grained Ferrite Network and Coarse Pearlite Matrix, Radial Surface



$N_{\frac{1}{2}} = 398$

Mag: 300X

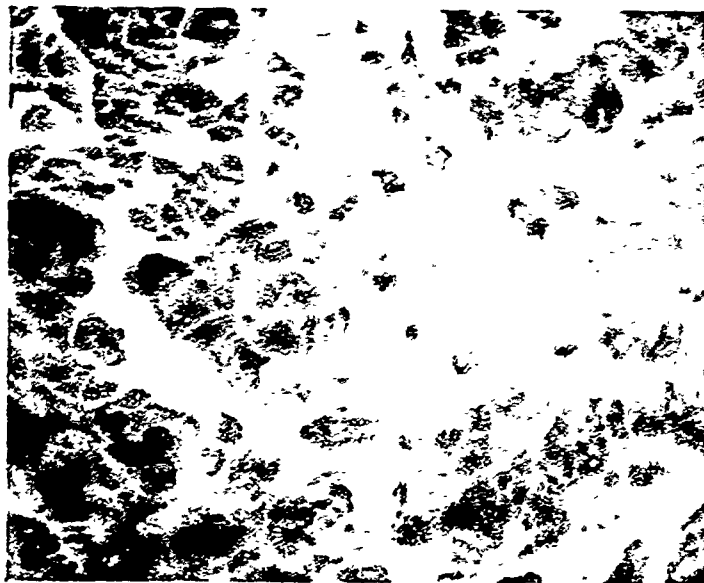
Figure 4. XF-1: Large Grained Ferrite Network and Coarse Pearlite Matrix (Same fragment as Figure 3, but an area closer to the center of the radial surface.)



$N_{\frac{1}{2}} = 256$

Mag: 300X

Figure 5. XF-1: Ferrite Network and Moderately Tempered Martensite Matrix, Axial Surface



$N_{\frac{1}{2}} = 256$

Mag: 3000X

Figure 6. XF-1: Ferrite Network and Moderately Tempered Martensite Matrix (Same as Figure 5, but higher magnification.)



$N_{\frac{1}{2}} = 115$

Mag: 1000X

Figure 7. Ferrite Network and Fine Pearlite Matrix,  
Radial Surface

## SEM of HF-1 Steel

The microstructure, hardness, and fragmentation performance of four selected conditions of HF-1 examined in this study are given in Table II. Two of these exhibited superior fragmentation performance. As with XF-1, the fragmentation performance is shown as  $N_{\frac{1}{2}}$  and represents an average of three tests. The differences in fracture modes of HF-1 as affected by differences in metallurgical structure are discussed below.

A typical radial fracture surface that was observed on fragments from one of the superior fragmenting conditions (a carbide network and lightly tempered martensite matrix microstructure) is shown in Figures 8 and 9. The fractographs indicate that intergranular separation was the only operable mode of fracture.

Table II.  
Fragmentation Performance of HF-1 Steel Cylinders With  
Selected Microstructures

<u>Structure</u>	<u>Hardness</u>	<u><math>N_{\frac{1}{2}}</math></u>
Carbide network and lightly tempered martensite matrix	Rc 44	468
Carbide network and fine pearlite matrix	Rc 30	458
Spheroidized	Rc 26	279
Homogenized at 2200° F, then heat treated to produce random carbides and patches of pearlite	Rc 30	193

The fracture morphology that was observed most generally on both radial and axial surfaces of fragments from the other superior condition (a carbide network and fine pearlite network) is shown in Figure 10. This fractograph, taken from an axial surface, indicates predominantly an intergranular separation mode similar to that observed for the structure with a martensite matrix. However, a secondary cracking, which was found more frequently on axial surfaces than on radial surfaces, is also shown. The major components of these cracks appear to be radially directed. In addition to intergranular separation, some tendency for transgranular cleavage was also observed for this structure. This is shown in Figure 11. Areas of cleavage can be seen quite readily at the

upper right and lower left hand corners of the figure. Note the flat facets and river patterns at these areas.

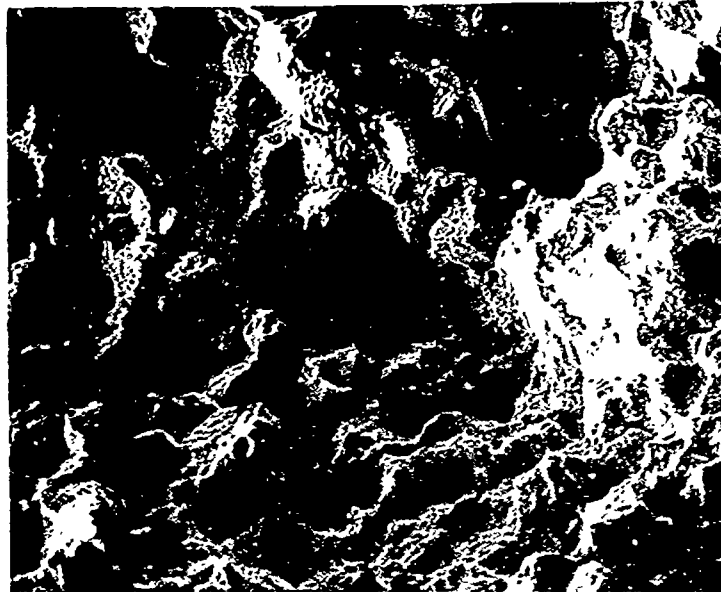
The fracture mode observed on both radial and axial surfaces of fragments with a spheroidized microstructure which provides intermediate fragmentation performance is shown in Figures 12 and 13. Fracture appears to be composed of a mixed mode of dimpled rupture and transgranular cleavage. Both modes occurred on a very fine scale and the river patterns on the cleavage facets were not well defined. This is especially evident in Figure 13. The radial surfaces of fragments in the spheroidized condition were quite rough as compared to the fragments with a carbide network previously described.

The poorest fragmenting condition noted for HF-1 was represented by a structure consisting of random carbides and patches of pearlite. A mixed mode of fracture, composed of transgranular cleavage and transgranular dimpled rupture, was observed on radial surfaces of fragments from cylinders in this condition. This is shown in Figure 14. The dimpled rupture in some areas occurred on a very fine scale as is shown in Figure 15. The radial fracture surfaces of fragments in this group were extremely rough in texture as compared to those of the fragments from the best fragmenting cylinders.

#### SEM of Fracture Surfaces Adjacent to Inner Walls of Cylinders

In the course of these studies, there was one common topographical feature observed in both alloys, regardless of whether the microstructure provided good or poor fragmentation. This feature was found on essentially all longitudinal fracture surfaces adjacent to and oriented at approximately  $45^\circ$  to the inner wall of the cylinder; that is, on fracture surfaces which were coincident with planes of maximum shear in an expanding cylinder. Macroscopically, these surfaces appeared planar, quite smooth, and highly reflective.

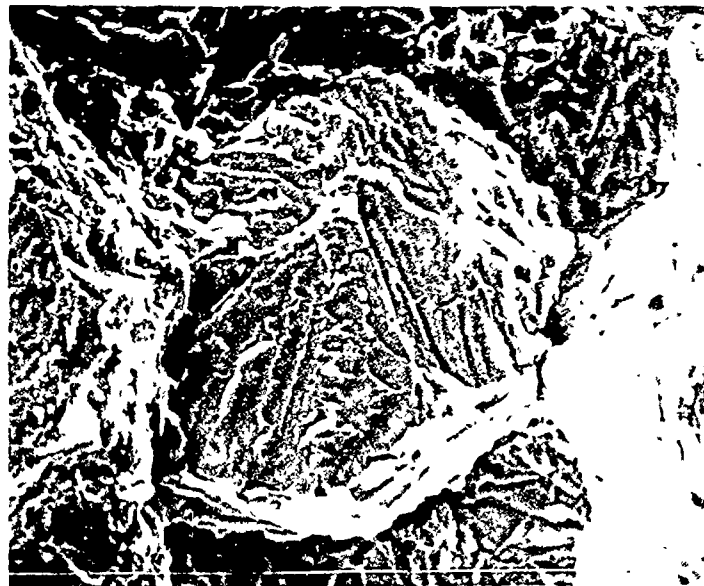
Figures 16 and 17 are typical high magnification fractographs of these shear-oriented planar surfaces. The topography is essentially featureless with the exception of appearing somewhat smeared; that is, no distinct failure mode such as intergranular failure, cleavage, or dimpled rupture could be identified in these regions.



$N_{\frac{1}{2}} = 525$

Mag: 180X

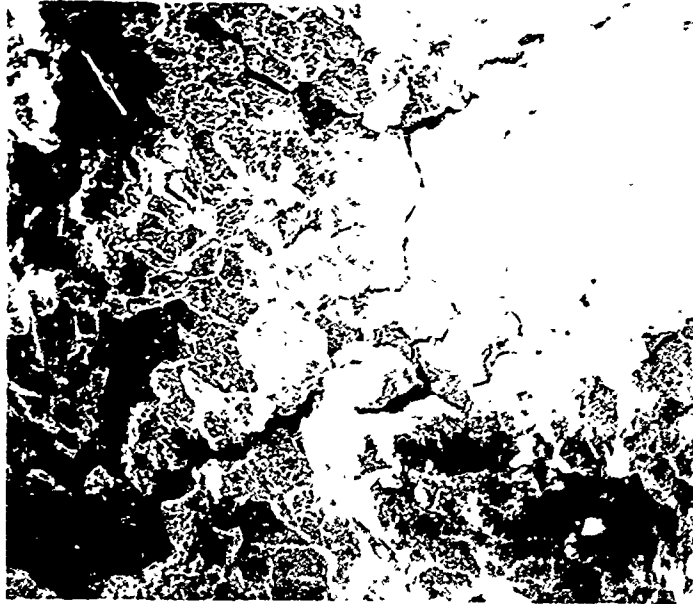
Figure 8. HF-1: Carbide Network and Lightly Tempered Martensite Matrix, Radial Surface



$N_{\frac{1}{2}} = 525$

Mag: 1000X

Figure 9. HF-1: Carbide Network and Lightly Tempered Martensite Matrix, Radial Surface (Same as Figure 8, but higher magnification.)



$N_{\frac{1}{2}} = 513$

Mag: 100X

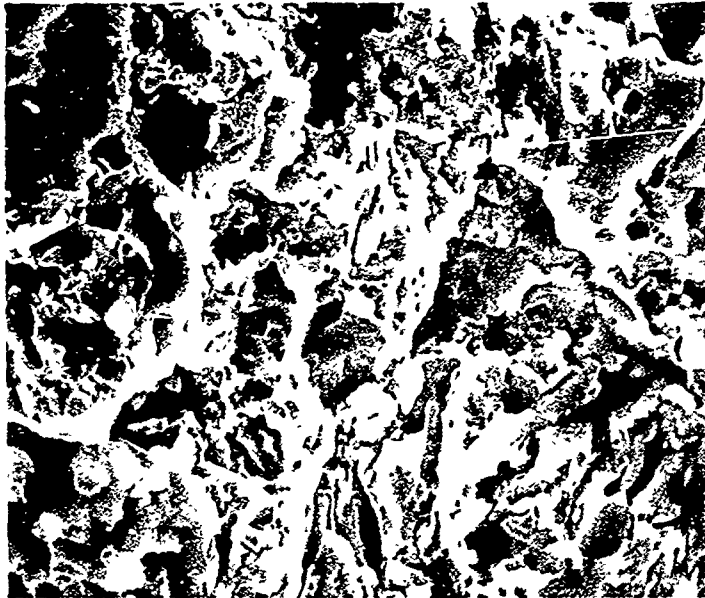
Figure 10. HF-1: Carbide Network and Fine Pearlite Matrix, Axial Surface



$N_{\frac{1}{2}} = 513$

Mag: 1000X

Figure 11. HF-1: Carbide Network and Fine Pearlite Matrix, Axial Surface (Same as Figure 10, but higher magnification.)



$N_{\frac{1}{2}} = 246$

Mag: 3000X

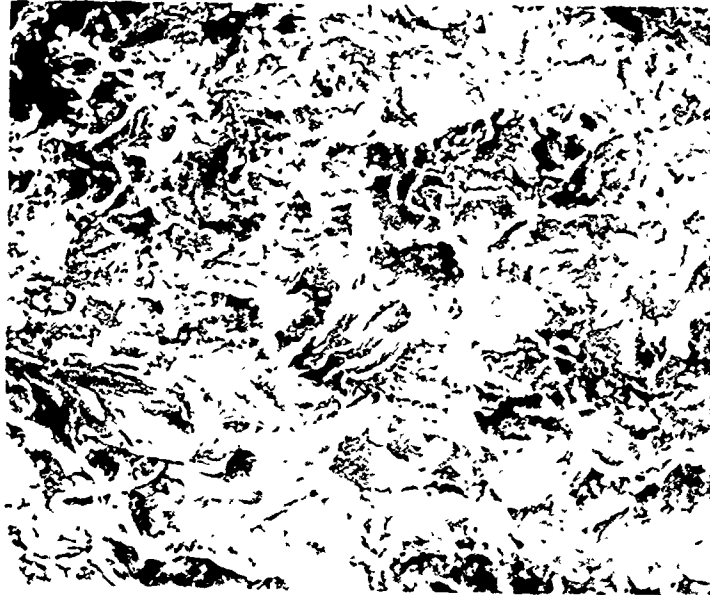
Figure 12. HF-1: Spheroidized, Radial Surface



$N_{\frac{1}{2}} = 246$

Mag: 10,000X

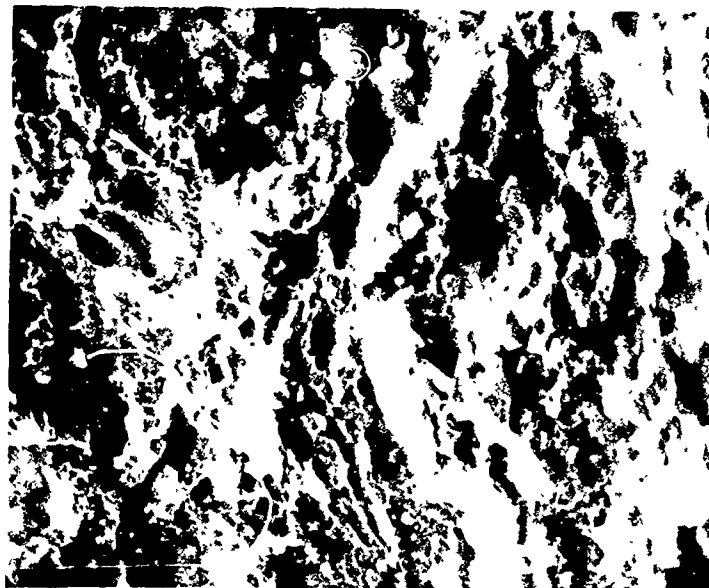
Figure 13. HF-1: Spheroidized, Radial Surface (Same as Figure 12, but higher magnification.)



$N_{\frac{1}{2}} = 174$

Mag: 1000X

Figure 14. HF-1: Homogenized at 2200° F; Then Heat-treated to Produce Random Carbides and Pearlite; Radial Surface



$N_{\frac{1}{2}} = 174$

Mag: 3000X

Figure 15. HF-1: Homogenized at 2200° F; Then Heat-treated to Produce Random Carbides and Pearlite; Radial Surface (Same as Figure 14, but higher magnification.)



$N_2 = 232$

Mag: 100X

Figure 16. HF-1: Partial Carbide Network and Spheroids in a Well Tempered Martensite Matrix, Shear Surface



$N_2 = 232$

Mag: 1000X

Figure 17. HF-1: Partial Carbide Network and Spheroids in a Well Tempered Martensite Matrix, Shear Surface (Same as Figure 16, but higher magnification.)

## DISCUSSION

### SEM of XF-1 Steel

The most important features which were observed on XF-1 steel by SEM were:

1. All three structures examined contained a ferrite network but exhibited quite different fracture modes. It is inferred from this that a ferrite network does not play a significant role in promoting dynamic brittle behavior.
2. Transgranular cleavage occurred in the two structures which contained pearlite; in both cases intergranular dimpled rupture accompanied the cleavage mode.
3. The cracks which promote radial fracture, at least in the coarse pearlite structure, are nucleated within the cylinder wall close to the outer surface of the cylinder.

In attempting to relate some of the above observations with the fragmentation performance of the steels shown in Table I, some inconsistencies became apparent. For example, the two structures which contained pearlite failed on radial surfaces predominantly by brittle transgranular cleavage. However, one of them exhibited the best fragmentation performance and the other exhibited the worst fragmentation performance. In contrast to this, a brittle mode was conspicuously absent in the structure which exhibited intermediate fragmentation performance. This structure contained tempered martensite and an intergranular dimpled rupture was observed along shear directions; radial fracture surfaces were not produced.

The fact that in studies of XF-1, a coarse pearlite matrix was found to produce the optimum fragmenting condition is consistent with previous studies on PR-2<sup>2</sup> and on AISI 9255<sup>3</sup>. For PR-2, it was found that a coarse pearlite structure provided superior fragmentation to a normalized or to a quenched and tempered martensite structure. For AISI 9255, it was also found that a coarse pearlite microstructure fragmented better than the same composition with a fine pearlite microstructure.

---

<sup>2</sup>P.V. Riffin, "Progress Report on High-Silicon Steels for Fragmentation," AMMRC, April 1968.

<sup>3</sup>P.V. Riffin and E. N. Kinas, "Fragmentation Behavior of Silicon Steel AISI 9255 Under Explosive Loading," Report PL 67-04, AMMRC, Sep 1967.

## SEM of HF-1 Steel

The most important features which were observed on HF-1 steel by SEM were:

1. Intergranular separation occurred only in structures which contained a carbide network. Therefore, contrary to the insignificant role of the ferrite network in XF-1, a carbide network in HF-1 is an important factor in promoting a brittle intergranular separation mode.

2. Transgranular cleavage also occurred in structures of HF-1 which contained pearlite, but not to the same extent as in pearlite structures of XF-1.

3. Ductile dimpled rupture was observed in both the spheroidized and homogenized structures. This mode was not found in the structures with a carbide network. The dimples probably nucleate at the random carbides in the spheroidized and homogenized microstructures.

The results of the fractographic study on HF-1 are consistent with the fragmentation data shown in Table II. It was observed that only the two structures containing a carbide network exhibited completely brittle fracture modes on radial surfaces. These structures had superior fragmentation characteristics. In the structure with a lightly tempered martensite matrix, the brittle mode was entirely intergranular separation. In the other structure with a fine pearlite matrix, brittle fracture occurred by a mixed mode consisting of transgranular cleavage as well as intergranular separation.

These results suggest that in the case of HF-1, dynamic brittle failure on radial surfaces can occur by two mechanisms which will be dependent on the matrix constituent as well as the grain boundary constituent. For example, in a structure with a brittle grain boundary carbide network and a hard rigid martensite matrix, intergranular separation should be the dominant fracture mode. For this structure it is assumed that crack nucleation occurs within the brittle carbide network. Crack propagation then proceeds along the carbide network because its resistance to propagation is relatively poor as compared to the resistance of the martensite matrix. The latter, because of its high strength and toughness, is extremely difficult to plastically deform or to cleave. On the other hand, in a structure with a brittle grain boundary constituent and a relatively soft and less tough matrix, such as pearlite, intergranular separation can be accompanied by a cleavage mode because pearlite is relatively easy to cleave. The factor which determines which mode will occur at a given time is the relative orientation of the grain boundary (carbide) and the cleavage plane (pearlite) with respect to the major component of the tensile stress.

## SEM of Fracture Surfaces Adjacent to Inner Walls of Cylinders

The shear-oriented fractures produced adjacent to the inner wall of each cylinder are apparently both composition and structure-insensitive for the steels used in this study. The fractographically smeared appearance of these surfaces is nondescriptive in terms of readily identifiable fracture modes. It is suggested that this essentially featureless topography could result from adiabatic shearing<sup>4,5,6</sup> during dynamic straining of the cylinder. An extremely large amount of plastic deformation can occur at the high temperatures experienced in an adiabatic shear zone, and could seemingly account for the smeared condition of a fracture surface through that zone. This extreme plastic shear state initiates at the inner wall of the cylinder and propagates toward the outer surface along planes of maximum shear.

For cylinders which experienced radial fracture, it is assumed that the adiabatic shear zones and inward-moving radial cracks propagated concurrently, and that ultimate fracture occurred as a result of their interaction.

## CONCLUSIONS

1. It has been demonstrated that SEM is well suited for studies of fracture surfaces produced by explosive loading.
2. The direct identification of microscopic fracture modes by SEM permits a less ambiguous association of these features with metallurgical structure than does optical metallography. The crack nuclei and fracture paths revealed in this work would, at best, be only implied by optical metallography.
3. In both the XF-1 and the HF-1 structures which exhibited the best fragmentation performance, radial fracture resulted primarily from a brittle mode of failure.
4. Brittle failure is a necessary, but not a sufficient, condition for superior fragmentation. That is, all of the structures which fragmented well exhibited brittle failure, but all the structures

---

<sup>4</sup>C. Zener and J. H. Hollomon, "Effect of Strain Rate Upon Plastic Flow of Steel," J. Appl. Phys. 15, 22 (1944).

<sup>5</sup>T. A. Read, H. Marcus, and J.M. McCaughey, "Plastic Flow and Rupture of Steel at High Hardness Levels," Fracturing of Metals, ASM, p.228 (1948).

<sup>6</sup>R. F. Recht, "Catastrophic Thermoplastic Shear," J. Appl. Mech 31, 189 (1964).

which exhibited brittle failure did not necessarily fragment well.

5. Shear oriented fracture surfaces are invariably formed adjacent to the inner surfaces of cylinders. Their topography suggests an association with adiabatic shearing.

#### RECOMMENDATIONS

It is recommended that additional studies, utilizing SEM, be conducted to correlate fracture mode and microstructure with fragmentation. It could be expected that such studies would provide a means of identifying the important parameters relating metallurgical structure with fragmentation performance.

#### REFERENCES

1. B. P. Bardes, "Mechanism of Fragmentation of Silico-Manganese Steels," Frankford Arsenal Report R-1918, March 1969.
2. P. V. Riffin, "Progress Report on High-Silicon Steels for Fragmentation," AMMRC, April 1968.
3. P. V. Riffin and E. N. Kinas, "Fragmentation Behavior of Silicon Steel, AISI 9255 Under Explosive Loading," Report PL 67-04, AMMRC, September 1967.
4. C. Zener and J. H. Hollomon, "Effect of Strain Rate Upon Plastic Flow of Steel," J. Appl. 15, 22 (1944).
5. T. A. Read, H. Marcus, and J. M. McCaughey, "Plastic Flow and Rupture of Steel at High Hardness Levels," Fracturing of Metals, ASM, p. 228 (1948).
6. R. F. Recht, "Catastrophic Thermoplastic Shear," J. Appl. Mech 31, 189 (1964).

DISTRIBUTION

Hq, Office of Rsch & Development  
Attn: Dr. T. Sullivan  
CRD-PES  
3045 Columbia Pike, Highland Bldg  
Arlington, VA 22204

Hq, U.S. Army Materiel Command  
Washington, DC 20315  
2 Attn: Chief Scientist, AMCDL-CS  
1 Attn: Director, Research, Develop-  
ment & Engineering - AMCRD  
1 Attn: Dr. R. B. Dillaway  
Deputy for Laboratories,  
AMCDL

1 Attn: AMCRD-RS  
1 Attn: Mr. Rackowski  
AMCRD-DE-W  
1 Attn: Mr. L. Croan  
AMCRD-TC, Bldg T-7

U.S. Army Munitions Command  
Dover, NJ 07801  
1 Attn: Director, Research,  
Development, Engineering  
1 Attn: Mr. Chesnov, AMSMU-RE-R  
4 Attn: CDC Liaison Officer  
AMSMU-LN-CD  
1 Attn: USMC Liaison Officer  
AMSMU-LN-MC

Commanding Officer (2)  
Technical Library, Bldg 313  
Aberdeen Proving Ground, MD 21005

Commanding Officer  
Picatinny Arsenal  
Dover, NJ 07801

2 Attn: Scientific & Technical  
Information Branch

1 Attn: R. Benner, SMUPA-VP  
1 Attn: K. Bramble, SMUPA-DW  
1 Attn: E. N. Clark, SMUPA-VC  
1 Attn: B. Farbanish, SMUPA-DA  
1 Attn: B. A. Konrad, SMUPA-DA

Commanding Officer  
Harry Diamond Laboratories  
Attn: AMXDO TIB  
Washington, DC 20438

Defense Documentation Center (2)  
Cameron Station  
Alexandria, VA 22314

Federal Aviation Administration  
Attn: Administrative Standard  
Division (MS-110)  
800 Independence Ave., S.W.  
Washington, DC 20590

Commanding Officer  
A. F. Armament Laboratories  
Eglin AFB, FL 32542

1 Attn: DLOS  
1 Attn: E. A. Wintermoyer  
AFATL (ATRO)

Commanding Officer  
Lake City Army Ammunition Plant  
2 Attn: Mr. G. E. Ellis, SMULC-IE  
Independence, MO 64056

Commanding Officer  
Army Research & Development Center  
Aberdeen Proving Ground, MD 21005  
1 Attn: A. M. Dietrich, AMXRD-BRL  
1 Attn: S. Kronman, AMXRD-BRL  
1 Attn: D. Waldon, AMXRD-AWA  
1 Attn: C. Glass, AMXRD-BRL

Commanding Officer  
U. S. Army Tropic Test Center  
Attn: STETC-MO-A (Technical Ly)  
Drawer 942  
Fort Clayton, Canal Zone 09827

Hq, U. S. Army Materials &  
Mechanics Research Center  
Watertown, MA 02172  
1 Attn: Technical Information Div  
1 Attn: Mr. P. Riffin

Commanding Officer  
U. S. Army Research Office-Durham  
Durham, NC 27706  
1 Attn: Dr. J. Dawson  
1 Attn: Dr. H. Davis

Chief, Office of Naval Research  
Department of the Navy  
Washington, DC 20360

Mr. Forrest Williams-MAN  
Aero Materials Division  
Naval Air Development Center  
Johnsville, Warminster, PA  
18974

Commander  
U. S. Naval Weapons Center  
Attn: Mr. J. Pearson  
China Lake, CA 93555

Commander  
U. S. Naval Weapons Laboratory  
Attn: Mr. R. W. Lowry  
Dahlgren, VA 22448

Frankford Arsenal:

1 Attn: Commander's Reading  
File, H1210/107-B

1 Attn: Technical Director  
A1000/107-1

1 Attn: Plans Branch, U1000/107-2

1 Attn: G. White, L1000/64-4

1 Attn: Reliability Engineering  
Branch, Q3100/219-3

1 Attn: Patent Branch, R1000/519

2 Attn: Library, K2400/51-2  
(1 - Reference copy  
1 - Circulation copy)

1 Attn: Project File, L3200/64-4

2 Attn: J. B. Corrie, L3200/64-4

10 Attn: W. B. Steward, L3200/149-1

1 Attn: J. C. Beetle, L3200/149-1

1 Attn: H. Markus, L3000/64-4

Frankford Arsenal - Cont'd

1 Attn: D. H. Kleppinger, L3100/149-2

1 Attn: A. Gallaccio, L3300/64-2

1 Attn: B. W. Bushey, T1000/220-2

1 Attn: R. A. Meinert, T3300/220-2

1 Attn: C. E. Sallade, T4100/220-2

6 Attn: Technical Reports Editing  
Branch, K2200/64-3

Printing & Reproduction Division  
FRANKFORD ARSENAL  
Date Printed:9/18/72

UNCLASSIFIED

Security Classification

DOCUMENT CONTROL DATA - R & D

(Security classification of title, body of abstract and indexing annotation must be entered when the overall report is classified)

1. ORIGINATING ACTIVITY (Corporate author) FRANKFORD ARSENAL Philadelphia, PA 19137		2a. REPORT SECURITY CLASSIFICATION UNCLASSIFIED	
		2b. GROUP N/A	
3. REPORT TITLE A FRACTOGRAPHIC INVESTIGATION OF EXPLOSIVELY FRAGMENTED SILICON-MANGANESE STEELS BY SCANNING ELECTRON MICROSCOPY			
4. DESCRIPTIVE NOTES (Type of report and inclusive dates) Technical research memorandum			
5. AUTHOR(S) (First name, middle initial, last name) JAMES C. BEETLE WILLIAM B. STEWARD			
6. REPORT DATE May 1972	7a. TOTAL NO. OF PAGES 32	7b. NO. OF REFS 6	
8a. CONTRACT OR GRANT NO. AMCMS Code: 502E.11.09900	9a. ORIGINATOR'S REPORT NUMBER(S) F.A. Report M72-11-1		
b. PROJECT NO. DA Project: 1T062105A039	9b. OTHER REPORT NO(S) (Any other numbers that may be assigned this report)		
c.			
d.			
10. DISTRIBUTION STATEMENT Distribution limited to U.S. Government agencies only - Test and Evaluation, May 1972. Other requests for this document must be referred to the Commanding Officer, Frankford Arsenal, Phila., Pa., Attn: SMUFA-3200.			
11. SUPPLEMENTARY NOTES		12. SPONSORING MILITARY ACTIVITY AMCRD-T	
13. ABSTRACT The influence of microstructure upon fracture mode and relative fragmentation performance of steel test cylinders was assessed fractographically by scanning electron microscopy. For the compositions used in this study, a microstructural constituent which provides a path for brittle fracture under dynamic conditions appears to be a necessity for enhanced fragmentation.			

DD FORM 1473

NOV 68

REPLACES DD FORM 1473, 1 JAN 64, WHICH IS OBSOLETE FOR ARMY USE.

UNCLASSIFIED

Security Classification

UNCLASSIFIED

Security Classification

14 KEY WORDS	LINK A		LINK B		LINK C	
	ROLE	WT	ROLE	WT	ROLE	WT
Fracture Fragmentation Scanning Electron Microscope Microstructure High-Fragmenting Steel						

UNCLASSIFIED

Security Classification